Supplemental Material: Role of Advective Inertia in Active Nematic Turbulence

Colin-Marius Koch and Michael Wilczek*
Max Planck Institute for Dynamics and Self-Organization, Am Faßberg 17, 37077 Göttingen, Germany and Faculty of Physics, Georg-August-Universität Göttingen, Friedrich-Hund-Platz 1, 37077 Göttingen, Germany

NONDIMENSIONALIZATION OF THE EQUATIONS OF MOTION

For the comparison of parameter choices investigated in this paper and in previous literature, we obtain in the following the set of nondimensional equations stated in the main text by rescaling length, time, and mass with the nematic scales l_n, t_n, and m_n, respectively. We first state the dimensional equations of motion, then motivate the nematic scales and rescale the equations with them. We finally identify the dimensionless numbers and discuss the meaning of this particular choice of nondimensionalization.

Dimensional Equations of Motion

The Navier-Stokes equation we use to model a 2D active nematic (as adapted from [1], see also [2]) is:

$$\begin{aligned} \nabla \cdot \boldsymbol{u} &= 0\,, \\ \rho(\partial_t \boldsymbol{u} + \boldsymbol{u}\cdot\nabla\boldsymbol{u}) &= -\nabla p + \eta\Delta\boldsymbol{u} + \nabla\cdot(\boldsymbol{\sigma}_e - \boldsymbol{\sigma}_a) - \mu\boldsymbol{u}\,, \\ \boldsymbol{\sigma}_e &= -\lambda S\boldsymbol{H} + \boldsymbol{H}\boldsymbol{Q} - \boldsymbol{Q}\boldsymbol{H}\,, \\ \boldsymbol{\sigma}_a &= \alpha\boldsymbol{Q}\,, \end{aligned} \tag{1}$$

where $\boldsymbol{u}$ is the velocity and p is the pressure; $\boldsymbol{\sigma}_e$ and $\boldsymbol{\sigma}_a$ are the elastic and active stresses, respectively, and $\boldsymbol{H}$ is the molecular tensor defined as the functional derivative of the free energy:

$$\begin{aligned} \boldsymbol{H} &= K\Delta\boldsymbol{Q} - C\boldsymbol{Q}(S^2-1) = -\frac{\delta\mathcal{F}}{\delta\boldsymbol{Q}}\,, \\ \mathcal{F} &= \int d^2\boldsymbol{x}\,\left[\frac{K}{2}(\partial_i Q_{jk})^2 + \frac{C}{2}((Q_{ij}\,Q_{ji})^2 - Q_{ij}\,Q_{ji})\right]\,, \\ S &= \sqrt{2\,Q_{ij}\,Q_{ji}}\,. \end{aligned} \tag{2}$$

Note that we only consider extensile stresses in this work, i.e. we choose $\alpha > 0$ and write a negative sign in front of the active stress. The time evolution for the alignment tensor is given by:

$$\begin{aligned} \partial_t\boldsymbol{Q} + \boldsymbol{u}\cdot\nabla\boldsymbol{Q} &= \lambda S\boldsymbol{E} - \boldsymbol{W}\boldsymbol{Q} + \boldsymbol{Q}\boldsymbol{W} + \gamma^{-1}\boldsymbol{H}\,, \\ E_{ij} &= \frac{1}{2}(\partial_i u_j + \partial_j u_i)\,, \\ W_{ij} &= \frac{1}{2}(\partial_i u_j - \partial_j u_i)\,. \end{aligned} \tag{3}$$

The definition of the parameters can be found in Table S1.

Nematic Scales

For our nondimensionalization we use the nematic length, time, and mass scales

$$l_n = \sqrt{\frac{K}{C}}\,, \qquad t_n = \frac{\gamma}{C}\,, \quad \text{and} \quad m_n = \frac{\gamma^2}{C}\,, \tag{4}$$

which are defined with respect to parameters controlling the relaxation towards a uniformly aligned state. Namely, these are the elastic constant K, the material constant C, and the rotational viscosity γ, which control the orientational diffusion, alignment, and damping of $\boldsymbol{Q}$ in Eqs. (2) and (3), respectively.

The nematic length scale l_n can be understood to be proportional to the defect core radius when the system is deep in the nematic regime [3]. From observing the vorticity and nematic order parameter fields, defects seem to be the smallest visible structures in the active nematic turbulent state (Fig. S1 and Fig. 1 in the main text). To resolve their scales properly, it is reasonable to use the nematic length scale for measuring length scales in the system.

The nematic time scale $t_n = \gamma\, l_n^2/K$ can be thought of as the time scale over which distortions in the orientational field relax to uniform alignment on length scales l_n [3]. It may therefore be accessible experimentally as a characteristic scale in the system without activity.

For the nematic mass, motivation from observations is more difficult. However, choosing the same parameters appearing in the nematic length and time scales, our definition of the nematic mass is consistent and unique.

Rescaling the Equations of Motion

In the following, we rescale all fields with the nematic length, time, and mass scales defined in the previous section. For conciseness, we additionally use the velocity $u_n = l_n/t_n$. The nondimensional variables are denoted with an asterisk (in the main text and the following sections, the asterisk is dropped).
The velocity, as well as spatial and temporal derivatives, are:

$$\boldsymbol{u} = u_n\,\boldsymbol{u}^*\,,\ \nabla = \frac{1}{l_n}\nabla^*\,,\ \Delta = \frac{1}{l_n^2}\Delta^*\,,\ \partial_t = \frac{1}{t_n}\partial_{t^*}\,. \tag{5}$$

To rescale the pressure one typically chooses one of the following two options [4, p. 92]:

$$\frac{p}{\rho} \equiv \bar{p} = u_n^2\,\bar{p}^* \qquad \text{or} \qquad \frac{p}{\eta} \equiv \tilde{p} = \frac{1}{t_n}\,\tilde{p}^*\,, \tag{6}$$

whereby the first option is used for flows in which inertia dominates and the latter for flows in which viscous dissipation dominates. Because the pressure gradient accounts for the incompressibility of the flow, it has to remain in the equations of motion even in the limit of inertia being negligible compared to dissipation, or vice versa. Hence, both choices for the pressure aim at balancing the larger term against the pressure gradient. Here, expecting experimentally a dominance of viscous dissipation, we use the option in which pressure is rescaled with viscosity.
We split the elastic stress for clarity in two nondimensional contributions, $\boldsymbol{\sigma}_K^*$ and $\boldsymbol{\sigma}_C^*$, which are subscripted with their prefactors K and C. In addition, we identify the nondimensional active stress $\boldsymbol{\sigma}_a^*$ as the alignment tensor $\boldsymbol{Q}$ with the activity parameter α as prefactor:

$$\boldsymbol{\sigma}_e = \frac{K}{l_n^2}\left[-\lambda S\Delta^*\boldsymbol{Q} + (\Delta^*\boldsymbol{Q})\boldsymbol{Q} - \boldsymbol{Q}(\Delta^*\boldsymbol{Q})\right] + C\lambda S\boldsymbol{Q}(S^2-1) = \frac{K}{l_n^2}\boldsymbol{\sigma}_K^* + C\boldsymbol{\sigma}_C^*\,, \tag{7}$$

$$\boldsymbol{\sigma}_a = \alpha\boldsymbol{Q} = \alpha\boldsymbol{\sigma}_a^*\,. \tag{8}$$

The evolution equations (1) and (3) with nondimensionalized variables then read:

$$\rho\left(\frac{u_n}{t_n}\,\partial_{t^*}\boldsymbol{u}^* + \frac{u_n^2}{l_n}\,\boldsymbol{u}^*\cdot\nabla^*\boldsymbol{u}^*\right) = -\frac{\eta}{t_n\,l_n}\,\nabla^*\tilde{p}^* + \frac{\eta\,u_n}{l_n^2}\,\Delta^*\boldsymbol{u}^* + \frac{1}{l_n}\nabla^*\cdot\left[\frac{K}{l_n^2}\boldsymbol{\sigma}_K^* + C\boldsymbol{\sigma}_C^* - \alpha\boldsymbol{\sigma}_a^*\right] - \mu\,u_n\,\boldsymbol{u}^*\,, \tag{9}$$

$$\frac{1}{t_n}\,\partial_{t^*}\boldsymbol{Q} + \frac{u_n}{l_n}\boldsymbol{u}^*\cdot\nabla^*\boldsymbol{Q} = \frac{u_n}{l_n}\lambda S\boldsymbol{E}^* - \frac{u_n}{l_n}\boldsymbol{W}^*\boldsymbol{Q} + \frac{u_n}{l_n}\boldsymbol{Q}\boldsymbol{W}^* + \frac{K}{\gamma\,l_n^2}\Delta^*\boldsymbol{Q} - \frac{C}{\gamma}\boldsymbol{Q}(S^2-1)\,. \tag{10}$$

Until here, the specific choice of length, time, and mass scales did not matter. However, now we can simplify the expressions by using our definitions of the nematic scales based on the parameters (4) and obtain:

$$\frac{\rho\,u_n\,l_n}{\eta}(\partial_{t^*}\boldsymbol{u}^* + \boldsymbol{u}^*\cdot\nabla^*\boldsymbol{u}^*) = -\nabla^*\tilde{p}^* + \Delta^*\boldsymbol{u}^* + \frac{K}{\eta\,u_n\,l_n}\nabla^*\cdot\left[\boldsymbol{\sigma}_e^* - \frac{\alpha\,l_n^2}{K}\boldsymbol{\sigma}_a^*\right] - \frac{\mu\,l_n^2}{\eta}\boldsymbol{u}^*\,, \tag{11}$$

$$\partial_{t^*}\boldsymbol{Q} + \boldsymbol{u}^*\cdot\nabla^*\boldsymbol{Q} = \lambda S\boldsymbol{E}^* - \boldsymbol{W}^*\boldsymbol{Q} + \boldsymbol{Q}\boldsymbol{W}^* + \Delta^*\boldsymbol{Q} - \boldsymbol{Q}(S^2-1)\,, \tag{12}$$

where we write now the nondimensional elastic stress $\boldsymbol{\sigma}_e^* = \boldsymbol{\sigma}_K^* + \boldsymbol{\sigma}_C^*$. This equation leaves us with four dimensionless prefactors (plus the nondimensional flow alignment parameter λ) which we define as the four dimensionless numbers

$$\mathrm{Re}_n = \frac{\rho\,u_n\,l_n}{\eta}\,, \qquad \mathrm{Er} = \frac{\eta\,u_n\,l_n}{K}\,, \qquad R_a = \frac{l_n^2}{l_a^2}\,, \quad \text{and} \quad R_f = \frac{l_n^2}{l_f^2}\,. \tag{13}$$

We call Re_n the microscopic (nematic) Reynolds number, Er the Ericksen number, R_a the active number, and R_f the friction number. The latter two are ratios of length scales:

$$l_n = \sqrt{\frac{K}{C}}\,, \qquad l_a = \sqrt{\frac{K}{\alpha}}\,, \qquad l_f = \sqrt{\frac{\eta}{\mu}}\,, \tag{14}$$

where l_n is the nematic, l_a is the active, and l_f is the friction length scale [1].
Thus, by choosing the nematic scales to nondimensionalize the equations of motion, we effectively reduced the number of free parameters from seven to four (not counting the flow alignment parameter λ).
Note at this point that the above-defined Reynolds and Ericksen numbers are defined via the nematic length and time scales. Different definitions of these numbers are possible, which means that the values of these numbers can be interpreted only in relation to the scales used to define them (see discussion below).

Discussion of the Nondimensionalization

In this study, we choose to nondimensionalize the equations of motion with the nematic scales. Different scales can be used which will result in different prefactors than the ones identified in the last section. A particular and useful choice is based on scales that are representative of the actual characteristic scales in the problem, which allows predicting whether one term in the equations of motion dominates over another. We will call this particular choice of scales the characteristic scales in the following. Using the characteristic scales, each term in the equations of motion is normalized, i.e. it takes values of order one. For example, if we assume the nematic scales to be the characteristic scales, the nonlinear advection $\boldsymbol{u} \cdot \nabla \boldsymbol{u}$ without its prefactor Re_n as well as the viscous diffusion $\Delta \boldsymbol{u}$ would be of order one. The microscopic Reynolds number Re_n then characterizes how strong nonlinear advection contributes to the time evolution compared to viscous diffusion. Depending on the actual value of the characteristic scales, the Reynolds number may be very small. In this case, nonlinear advection would contribute only little to the dynamics and could be neglected, justifying a low-Reynolds-number approximation. However, the nematic scales used in the nondimensionalization shown above are not characteristic scales and do not necessarily normalize each term in the equations of motion. Hence, no a priori information can be used to simplify the equations of motion.

In 2D active nematic turbulence, the characteristic scales of the flow and the orientational field are a priori unknown. While individual constituents, such as microtubule proteins, may define a specific microscopic length scale, the flow and orientational fields are excited on much larger scales, presumably better defined by the topological defects in the system. It is, therefore, questionable to apply the low-Reynolds-number approximation without the knowledge of the characteristic scales. The result can be, as has been shown in this paper, that parameter ranges are chosen which excite the flow strongly enough so that the low-Reynolds-number approximation becomes invalid.

Note that the microscopic Reynolds number, which we identified above as the prefactor of the inertial terms, is not the only Reynolds number that can be defined. In the main text, for instance, we compute the turbulent Reynolds number $\mathrm{Re}_t = \sqrt{E_{\mathrm{tot}}}\, l_i/\nu$, where $\nu = \eta/\rho$ is the kinematic viscosity and l_i is the integral length scale defined via the longitudinal velocity correlation function [5, p. 197]:

$$l_i = \int_0^\infty dr\, \frac{\langle u_x(\boldsymbol{x} + r\boldsymbol{e}_x, t)\, u_x(\boldsymbol{x}, t)\rangle}{\langle u_x(\boldsymbol{x}, t)^2\rangle}\,, \tag{15}$$

which characterizes the flow field based on the emerging velocities and the scale over which velocities are correlated.

PARAMETERS, EQUILIBRATION TO STATISTICALLY STATIONARY STATES, AND ONSET OF ACTIVE NEMATIC TURBULENCE

The parameters used in this paper are listed in Table S1. As with any numerical simulation, the physical dimensions, i.e. units, need to be specified such that a comparison to a real physical system becomes possible. Here, we specify all parameters in terms of the nematic scales defined above, i.e. the nematic length l_n, time t_n, mass m_n, and velocity $u_n = l_n/t_n$. The values listed in Table S1 are the rescaled ones, where the numerical values in simulation units can be obtained by using $l_n = 0.05, t_n = 0.025, m_n = 0.25$. Since numerical values for continuum-model parameters are not consistent throughout studies of active nematic turbulence, we compare our parameter values to a selection of other papers (Table S2).

We performed numerical simulations on a periodic domain of size $L = N_x \Delta x$. In order to study the statistics independent of the initial conditions, we equilibrated the system until it reached a statistically stationary state before analyzing the data. For $L = 204.8$ we first ran simulations at a lower resolution $N_{x,\mathrm{eq}} = 256$, $\Delta x_{\mathrm{eq}} = 0.8$ to equilibrate the system for $N_{t,\mathrm{eq}} = 5 \times 10^5$ time steps with $\Delta t_{\mathrm{eq}} = 8 \times 10^{-3}$. We then upscaled and equilibrated the simulations to the final resolution $N_x = 512$, $\Delta x = 0.4$ to resolve all spectral statistics well. We followed an analogous procedure to equilibrate the larger box size $L = 819.2$ with $N_x = 2048$.

We define the onset of active nematic turbulence within our investigated parameter range as the value of activity for which topological defects are first created (Fig. S1).

Parameter	Description	Numerical Value	Dimensions
ρ	Solvent density	0.01	$[m_n]\,[l_n]^{-2}$
		Figs. 4, S5: $0.01 \to 1$	
η	Solvent viscosity	0.1	$[m_n]\,[t_n]^{-1}$
		Figs. 4, S5: $0.01 \to 1$	
K	Elastic constant	1.0	$[m_n]\,[u_n]^2$
C	Material constant	1.0	$[m_n]\,[t_n]^{-2}$
γ	Rotational viscosity	1.0	$[m_n]\,[t_n]^{-1}$
λ	Alignment parameter	0.1	–
α	Activity	$0.025 \to 0.25$	$[m_n]\,[t_n]^{-2}$
μ	Linear friction coefficient	$0.0, 7.5 \times 10^{-5}$	$[m_n]\,[l_n]^{-2}\,[t_n]^{-1}$
		Figs. 4, S5: $7.5 \times 10^{-5} \to 7.5 \times 10^{-4}$	
		Figs. S3, S4: $7.5 \times 10^{-6} \to 7.5 \times 10^{-3}$	
Δx	Grid spacing	0.4	$[l_n]$
Δt	Time step size	0.002	$[t_n]$
N_x	Number of grid points	$512, 2048$	–
L	Box size	$204.8, 819.2$	$[l_n]$

TABLE S1. Model and simulation parameters as well as their values. Dimensions are defined via the nematic mass m_n, length l_n, and time t_n. These parameters were used in the numerical code and are equivalent to the nondimensional numbers shown in Table S2.

	Re_n	Er	R_a		R_f	L	N_x	Δx
This paper (Figs. 1-3)	0.1	0.1	0.025	$\to$ 0.25	$0.0, 7.5 \times 10^{-4}$	204.8	512	0.4
Giomi [1]	0.1	0.1	0.05	$\to$ 2.5	–	200	256	0.78
Hemingway et al. [3] Model 1	0.1	0.1	10	$\to$ 10^3	–	128	128	1.0
Hemingway et al. [3] Model 2	0	1.76	0.05	$\to$ 12.8	–	707	2048	0.35
Thampi et al. [6]	0.01	0.23	0.003	$\to$ 0.083	–	1095	400	2.74
Carenza et al. [7]	0.05	0.83	0.000625	$\to$ 0.0625	–	2290	512	4.47
Urzay et al. [8]	0.21	0.22	0.12	$\to$ 1.2	–	132	512	0.26

TABLE S2. Comparison of model parameters for various studies on active nematic turbulence with the same or similar (quasi-2D) model. Shown are the microscopic Reynolds number Re_n, the Ericksen number Er, the active number R_a, the friction number R_f as well as the box length L, the number of grid points N_x, and the grid spacing Δx. While most studies feature a larger parameter regime than displayed here, we chose for easier comparison only a subset of values corresponding to the respective main results. Similarly, in our work, Fig. 4 in the main text as well as Figs. S3–S5 cover a more extended parameter range than shown here, as specified in Table S1.

ENERGY AND ENSTROPHY BUDGET

The energy budget is the time evolution of the kinetic energy spectrum defined as

$$E(k,t) = \frac{1}{2\Delta k} \sum_{k \le |\boldsymbol{k}| < k+\Delta k} |\hat{\boldsymbol{u}}(\boldsymbol{k},t)|^2 \,, \tag{16}$$

where $\boldsymbol{k}$ is the wave vector, $\Delta k = 2\pi/L$, and the hat indicates the Fourier-transformed field. Contributions to the budget can be obtained term by term from the Navier-Stokes equation when taking the time derivative of the energy spectrum:

$$\partial_t E(k,t) = \frac{1}{\Delta k} \sum_{k \le |\boldsymbol{k}| < k+\Delta k} \Re\left[\hat{\boldsymbol{u}}^* \cdot \partial_t \hat{\boldsymbol{u}}\right] \tag{17}$$

$$= T + P + D + S_e + S_a + F \,, \tag{18}$$

where $\Re[\cdot]$ denotes the real part of the complex fields and the asterisk denotes the complex conjugate. The energy transfer $T(k,t)$ originates from the self-advection of the velocity and is responsible for a transfer of energy between

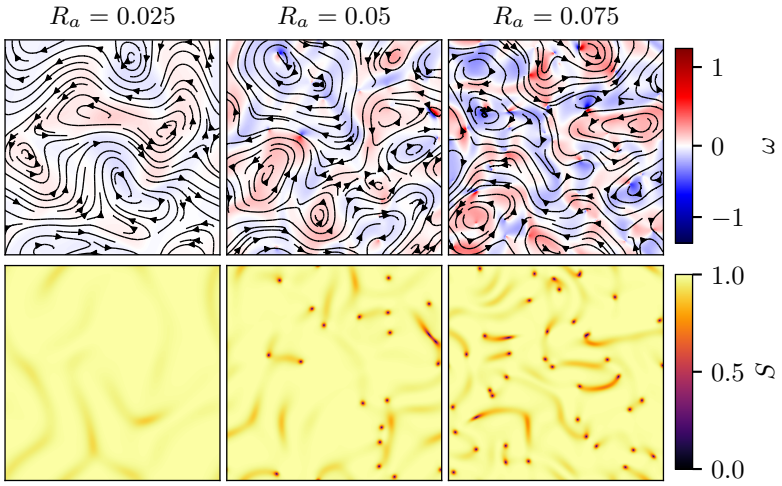

FIG. S1. Active stresses excite flows that distort the orientational field. For sufficiently large activities, pairs of defects form (corresponding to zero nematic order parameter), move through the system, and annihilate. We identify the onset of active turbulence close to $R_a = 0.05$ since this is the smallest investigated activity parameter for which we observe the emergence of defects. Top: vorticity (color map) and velocity (streamlines) for activities close to the onset of active nematic turbulence. Bottom: local nematic order parameter. ($L = 204.8$, $\mathrm{Re}_n = 0.1$, $\mathrm{Er} = 0.1$, $R_f = 0$)

the scales:

$$T(k,t) = \frac{1}{\Delta k} \sum_{k \le |\boldsymbol{k}| < k+\Delta k} \Re\left[\hat{\boldsymbol{u}}^* \cdot (-i\boldsymbol{k} \cdot \widehat{\boldsymbol{u}\boldsymbol{u}})\right] . \tag{19}$$

Its sum over all wave numbers is zero [9, p. 446]. The pressure contribution $P(k,t)$ is identical to zero on all scales for an incompressible flow:

$$P(k,t) = \frac{1}{\Delta k} \sum_{k \le |\boldsymbol{k}| < k+\Delta k} \Re\left[\hat{\boldsymbol{u}}^* \cdot \frac{1}{\mathrm{Re}_n}(-i\boldsymbol{k}\hat{p})\right] \tag{20}$$

$$= \frac{1}{\Delta k} \sum_{k \le |\boldsymbol{k}| < k+\Delta k} \Re\left[\frac{1}{\mathrm{Re}_n}(i\boldsymbol{k} \cdot \hat{\boldsymbol{u}})^* \hat{p}\right] \overset{\text{inc.}}{=} 0 . \tag{21}$$

Viscous dissipation extracts energy across scales and favors small scales due to its quadratic dependence on the wave number:

$$D(k,t) = \frac{1}{\Delta k} \sum_{k \le |\boldsymbol{k}| < k+\Delta k} \Re\left[\hat{\boldsymbol{u}}^* \cdot \frac{1}{\mathrm{Re}_n}(-k^2\hat{\boldsymbol{u}})\right] . \tag{22}$$

The elastic and active stress contributions to the budget depend on spatial variations in the orientational field $\boldsymbol{Q}$:

$$S_e(k,t) = \frac{1}{\Delta k} \sum_{k \le |\boldsymbol{k}| < k+\Delta k} \Re\left[\hat{\boldsymbol{u}}^* \cdot \frac{1}{\mathrm{Re}_n \mathrm{Er}}(i\boldsymbol{k} \cdot \hat{\boldsymbol{\sigma}}_e)\right] , \tag{23}$$

$$S_a(k,t) = \frac{1}{\Delta k} \sum_{k \le |\boldsymbol{k}| < k+\Delta k} \Re\left[\hat{\boldsymbol{u}}^* \cdot \frac{R_a}{\mathrm{Re}_n \mathrm{Er}}(-i\boldsymbol{k} \cdot \hat{\boldsymbol{\sigma}}_a)\right] . \tag{24}$$

Linear friction extracts energy proportional to the energy spectrum, i.e. primarily at scales of high energy:

$$F(k,t) = \frac{1}{\Delta k} \sum_{k \le |\boldsymbol{k}| < k+\Delta k} \Re\left[\hat{\boldsymbol{u}}^* \cdot \frac{R_f}{\mathrm{Re}_n}(-\hat{\boldsymbol{u}})\right] . \tag{25}$$

To complement the analysis of the energy budget, we also include an analysis of the enstrophy budget. The enstrophy

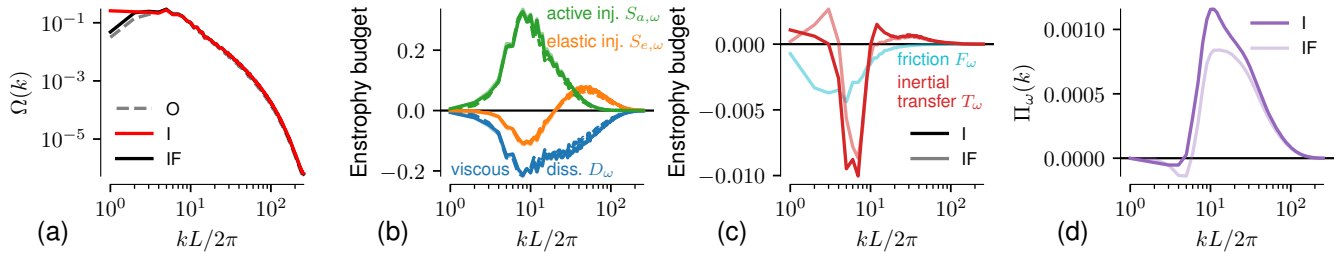

FIG. S2. Advective inertia mediates a direct enstrophy transfer to smaller scales. The original (O) regime is compared to the inertial (I) regime as well as to the regime with inertia and friction (IF): ensemble- and time-averaged (a) enstrophy spectrum $\Omega(k)$, (b) and (c) enstrophy budget contributions, (d) enstrophy flux $\Pi_\omega(k)$. ($L = 204.8$, $R_a = 0.2$, $\mathrm{Re}_n = 0.1$, $\mathrm{Er} = 0.1$, $R_f = 7.5 \times 10^{-4}$)

spectrum is defined as:

$$\Omega(k,t) = \frac{1}{2\Delta k} \sum_{k \le |\boldsymbol{k}| < k+\Delta k} |\hat{\omega}(\boldsymbol{k},t)|^2 \approx k^2 E(k,t)\,, \tag{26}$$

where the pseudo-scalar $\omega = \{\nabla \times \boldsymbol{u}\}_z$ is the vorticity. It is approximately proportional to the energy spectrum in the discrete case where the sum is over $k \le |\boldsymbol{k}| < k + \Delta k$ and exactly proportional in the continuous case where the sum is over $k = |\boldsymbol{k}|$. The enstrophy budget is defined analogously by differentiating the enstrophy spectrum with respect to time. Compared to the energy budget, it emphasizes effects on smaller scales (higher wave numbers) since it is effectively the energy budget multiplied with the wave number squared. For comparison, we have also evaluated the enstrophy budget from our simulations (Fig. S2). The enstrophy budget nicely demonstrates that the elastic stress also injects enstrophy (as well as energy) on smaller scales. It shows a direct enstrophy transfer towards smaller scales, which is similar to classical 2D turbulence. On top of that, it features a small inverse transfer of enstrophy towards larger scales.

FRICTION NUMBER PARAMETER SCAN

The results on the flow statistics (Fig. 3, main text) indicate that friction can compensate for inertial effects and return the system to a similar state as the one without inertia and friction. Therefore, we investigate how the flow statistics change with the friction number, R_f, and how they compare to the statistics in the original and inertial regimes (Fig. S3). As can be expected from the dissipative nature of the friction term, the kinetic energy and the turbulent Reynolds number decrease monotonically with increasing friction number [Figs. S3(b) and (d)]. Thereby, they show a smooth transition from the inertial to the original regime and beyond. The number of defects equally reaches the value of the original regime at intermediate R_f, but then decreases again for higher friction numbers [Fig. S3(a)]. The integral length scale also decreases monotonically [Fig. S3(c)], which coincides with a decrease in the flow structure size (Fig. S4).

These results suggest that the regime with inertia and friction can be qualitatively approximated by the original regime without inertia and friction if the friction number is tuned accordingly. Even though the flow statistics (Fig. S3) suggest also a good quantitative approximation, we observe that friction does not compensate the inertial transfer scale by scale in the energy budget (Fig. 2, main text). Quantitative differences in, e.g., the spectra are, therefore, to be expected. For example, friction has been shown to impact the slope of the energy spectrum in classical 2D turbulence [10].

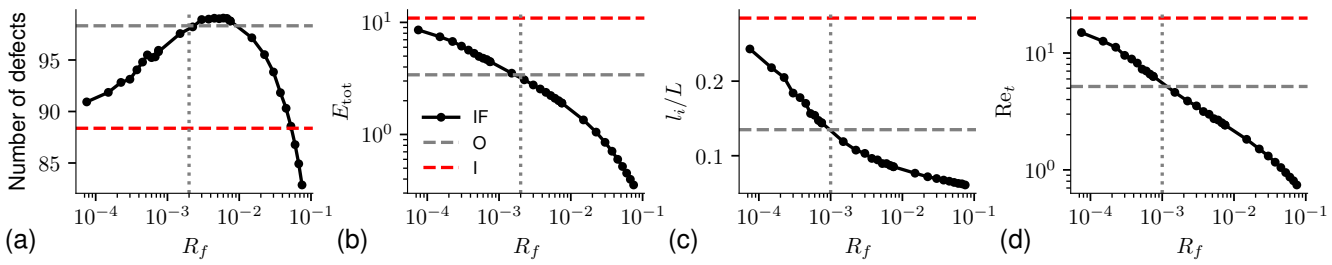

FIG. S3. Increasing the friction number R_f in the regime with inertia and friction (IF) dampens the flow statistics from the inertial (I) to the original (O) regime and beyond: ensemble- and time-averaged (a) number of defects, (b) total kinetic energy E_{tot}, (c) integral length l_i, (d) turbulent Reynolds number Re_t computed from (b) and (c). ($L = 204.8$, $R_a = 0.2$, $\mathrm{Re}_n = 0.1$, $\mathrm{Er} = 0.1$)

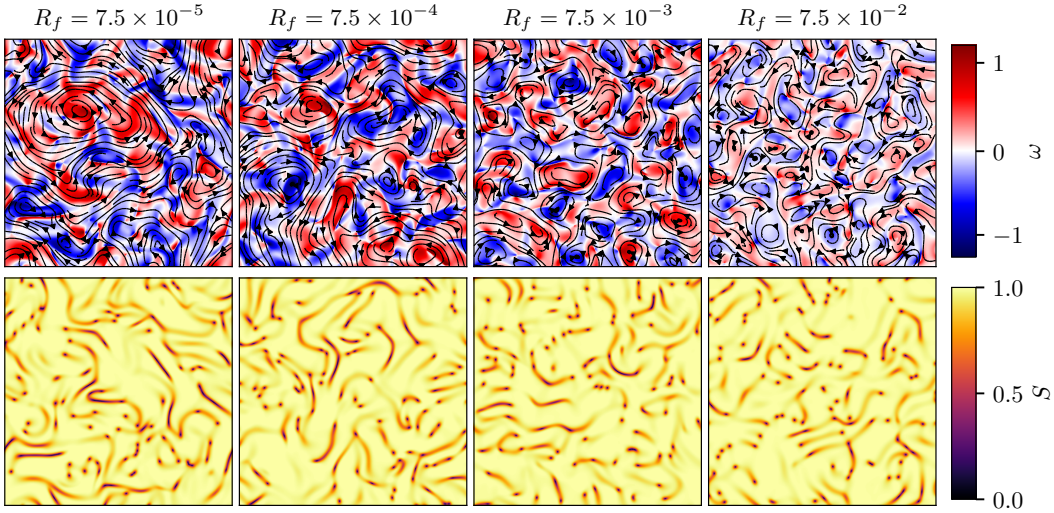

FIG. S4. Increasing the friction number R_f in the regime with inertia and friction visibly suppresses the large-scale flow field observed in the inertial regime. Top: vorticity (color map) and velocity (streamlines). Bottom: local nematic order parameter. ($L = 204.8$, $R_a = 0.2$, $\mathrm{Re}_n = 0.1$, $\mathrm{Er} = 0.1$)

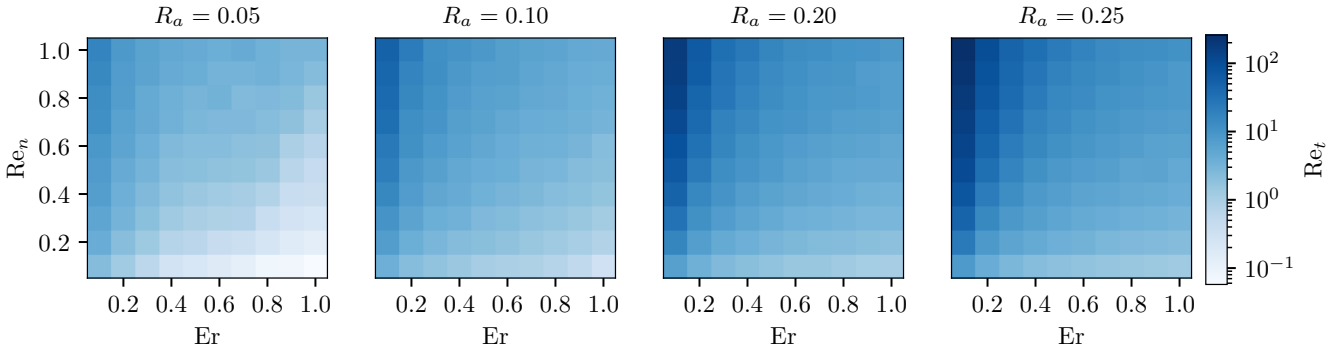

FIG. S5. The importance of inertia, quantified by the turbulent Reynolds numbers Re_t, increases directly with the microscopic Reynolds number Re_n and inversely with the Ericksen number. The simulations were performed in the regime with inertia and friction and were averaged over 30 independent random initial conditions. ($L = 204.8$, $R_f = 7.5 \times 10^{-4}$)

COMPARISON OF PARAMETER REGIMES

The nondimensionalization discussed in the sections above features, next to the active number R_a, the microscopic Reynolds and Ericksen numbers, Re_n and Er, respectively, which here depend on the nematic scales of the system. We scan a range of values for Re_n and Er for fixed R_a and measure the turbulent Reynolds number Re_t (Fig. S5), which provides a typical measure for the strength of inertial forces in turbulent flows. Extending the information of Fig. 4 in the main text, Fig. S5 includes parameter scans for two additional values of the active number R_a.

For all activities, the turbulent Reynolds number increases with increasing microscopic Reynolds number and decreasing Ericksen number. Depending on the active number R_a it takes values larger than unity even for small microscopic Reynolds numbers.

* michael.wilczek@ds.mpg.de

[1] L. Giomi, Phys. Rev. X **5**, 031003 (2015).
[2] For matrices $\boldsymbol{A}$ and $\boldsymbol{B}$ we use $\partial_j A_{ji}$ for $\nabla \cdot \boldsymbol{A}$ and $A_{ik}B_{kj}$ for $\boldsymbol{AB}$ in component notation.
[3] E. J. Hemingway, P. Mishra, M. C. Marchetti, and S. M. Fielding, Soft Matter **12**, 7943 (2016).
[4] D. Tritton, *Physical Fluid Dynamics* (Oxford: Oxford Science Publication, Clarendon Press, 1998).
[5] S. B. Pope, *Turbulent Flows* (Cambridge University Press, Cambridge, England, 2000).
[6] S. P. Thampi, R. Golestanian, and J. M. Yeomans, Phys. Rev. Lett. **111**, 118101 (2013).
[7] L. Carenza, L. Biferale, and G. Gonnella, Europhys. Lett. **132**, 44003 (2020).
[8] J. Urzay, A. Doostmohammadi, and J. M. Yeomans, J. Fluid Mech. **822**, 762 (2017).
[9] P. A. Davidson, *Turbulence: An Introduction for Scientists and Engineers* (Oxford University Press, New York, 2015).
[10] G. Boffetta, A. Cenedese, S. Espa, and S. Musacchio, Europhys. Lett. **71**, 590 (2005).